

## APPENDIX A

## BASIC ELEMENTS OF RADIO INTERFEROMETRY AND VLBI

There are four fundamental observables in the electromagnetic radiation fields of astronomical objects. They are the radiation intensity and polarization measured as a function of time and spectral frequency. Of particular importance to the understanding of the physical nature of an object are the absolute positions and relative spatial distributions of observables and the identification of distinct spatial features in the projected source brightness distribution. The angular resolution of a filled aperture telescope is limited by diffraction effects of the aperture,  $\theta_{\text{limit}} \approx \lambda/\text{diameter}$ . At radio wavelengths, the maximum angular resolution presently available on a single telescope is about 30 arcsec, i.e., the 100 m Bonn telescope at  $\lambda = 1.35$  cm and the FCRAO 13.7 m telescope at  $\lambda = 2$  mm. At  $\lambda = 18$  cm, the 300 m Arecibo telescope has a half-power beam width of 3 arcmin. Of course, optical observations that are limited only by tropospheric fluctuations resolve interesting spatial details far beyond the capability of any single radio telescope. Commensurate resolutions at radio wavelengths are clearly desirable. A case in point is the rapid time variations of

celestial masers. With the speed of light setting a lower limit on a disturbance travel time across the maser source and masers 100's to 1000's kiloparsec distant, the maser features must be substantially less than 1 arcsec in diameter.

The principles of interferometry have been successfully applied at radio wavelengths and attain angular resolutions routinely exceeding that of optical telescopes and in some cases as high as 0.0001 arcsec. Consider the filled aperture of a single telescope in terms of an array of adjacent elemental apertures  $\Delta x \Delta y$  in size. The far-field radiation pattern of the telescope  $F(l, m)$  is related to the aperture illumination field  $A(x, y)$  by the Booker-Clemmow theorem. That is,

$$F(l, m) = \sum_{\substack{i, k \\ \text{aperture}}} A(x_i, y_k) \exp[j 2 \pi (lx_i + my_k)] ,$$

where  $x$  and  $y$  are in units of wavelength and  $l$  and  $m$  are in radians. Thus the far-field radiation pattern is the sum of Fourier components in the far-field produced by pairs of elemental apertures at spacing  $\leq$  the telescope diameter. Clearly the far-field radiation pattern is confined to a solid angle determined by the maximum spacing of the elemental apertures. Or by reciprocity, each pair of elemental apertures sample a Fourier harmonic in the source spatial brightness distribution.

Let us consider the radiation field of a two-dimensional source brightness distribution,  $I(\theta_x, \theta_y)$ . For an  $I(\theta_x, \theta_y)$  radiating coherently across  $\theta_x, \theta_y$ , emission will be beamed into a power pattern of definite angular structure. For example, the case of thin screen scattering or a simple transmitting array of radiators.  $I(\theta_x, \theta_y)$  can be reconstructed by Fourier inversion of the radiation field intensities sampled spatially in the plane of the incident wavefront. However, coherent  $I(\theta_x, \theta_y)$  are limited to but a few cases in radio astronomy. For the most part, radio  $I(\theta_x, \theta_y)$ 's are combinations of statistically independent radiators. The spatial coherence of the radiation field of such a source can be sampled between increasing lateral separations in the plane of the incident wavefront. Of course, now the sampling technique must be phase stable. The spatial cross-correlation is  $\rho(u, v)$ , where  $u, v$  are the sampling baseline in the plane of the incident wavefront. The incoherent source brightness distribution,  $I(\theta_x, \theta_y)$ , and  $\rho(u, v)$  are Fourier transform pairs. The  $\rho(u, v)$  can be measured by a coherent two-element interferometer whose element separation projected into  $u, v$  samples at the spatial frequency  $(u^2 + v^2)^{1/2}$ . By physically moving the antennas and/or allowing the diurnal rotation of the earth to vary the aspect of the projected interferometer baseline in  $u, v$ ,  $\rho(u, v)$  can be sufficiently well determined such that its Fourier inversion represents a reasonable estimation of the true source brightness distribution.

#### A. Basic Interferometry

At a given epoch, a single Fourier component of  $I(\theta_x, \theta_y)$  is measured by a two-element interferometer. As the interferometer spacing is increased, Fourier components of higher order are observed. The phase stability of the simple two-element interferometer shown in Figure A.1 is maintained by using a common local oscillator and phase stable transmission lines. In Figure A.1, the incident wavefront arrives late at station #2 by the delay,

$$\tau_g = \frac{\lambda B}{c} \cos \theta$$

where  $B$  is the interferometer baseline in units of wavelength and  $\theta$  the source-baseline hour angle. The total power response of the interferometer is the product of signal #1 with the conjugate of signal #2 integrated over the system bandpass. Expressed as a complex quantity, the double sideband interferometer response for a point source is

$$R(t) = A(t) \cdot W(\tau_g - \tau_0) \exp(j\omega_{LO}(\tau_g - \tau_0)) ,$$

a simple harmonic fringe pattern under a 'white light' envelope,  $W(\tau_g - \tau_0)$ . The incremental tracking delay inserted in signal #2 is adjusted such that  $W(\tau_g - \tau_0) \approx 1$ . Note that the phase at the low

pass filter output,  $\omega_{LO} \tau_g$ , depends on  $\omega_{LO}$  rather than the sky frequency,  $\omega$ . This is a result of the incremental delay tracking the geometrical delay.

The interferometer baseline vector between any two stations at geocentric coordinates  $\phi_i, \lambda_i$  and geocentric radius,  $r_i$ , is  $\vec{B} = \vec{r}_2(\phi_2, \lambda_2) - \vec{r}_1(\phi_1, \lambda_1)$ , see Figure A.2(a). The source-baseline geometry, Figure A.2(b), is conveniently expressed in terms of their Greenwich Hour Angles (GHA) and declinations,  $L_s, \delta_s$  and  $L_B, \delta_B$ . The interferometer hour angle is defined as  $L = L_s - L_B$ . A detailed description of source-baseline geometry is included in Appendix B. The interferometer baseline vector projected into the plane of the incident wavefront, the  $u, v$  plane, is

$$u = B \cos \delta_B \sin L,$$

$$v = B(\sin \delta_B \cos \delta_s - \cos \delta_B \sin \delta_s \cos L),$$

where  $u$  is toward the east and  $v$  the north. The quantities  $u, v$  and  $B$  are expressed in units of wavelength. The geometrical interferometer delay for any source-baseline geometry is

$$\tau_g = \frac{\lambda B}{c} (\sin \delta_B \sin \delta_s + \cos \delta_B \cos \delta_s \cos L).$$

Consider a source brightness distribution which is extended over some small  $\bar{\rho}$  on the sky,  $I(\bar{\rho})$ , where  $\rho = [a_x^2 + a_y^2]^{1/2}$ ,  $a_x = (\alpha - \alpha_s) \cos \delta_s$ ,  $a_y = \delta - \delta_s$ , and  $\bar{\rho}$  is  $\perp$  to  $\hat{s}$ . Then the interferometer response is

$$\begin{aligned} R(t) &= \int_{\text{source}} d\bar{\rho} I(\bar{\rho}) \exp[j 2 \pi (\vec{B} \cdot \hat{s} + \vec{B} \cdot \bar{\rho})], \\ &= \exp(j 2 \pi \vec{B} \cdot \hat{s}) \\ &\quad \int d\theta_x d\theta_y I(\theta_x, \theta_y) \exp[j 2 \pi (u\theta_x + v\theta_y)]. \end{aligned}$$

The integral term is called the complex fringe visibility and represents the spatial coherence at  $u, v$  in the radiation field. Or alternatively,  $\gamma(u, v)$  is a measure of the amplitude and phase of that angular harmonic,  $k = [u^2 + v^2]^{-1/2}$ , of  $I(\theta_x, \theta_y)$ .  $\gamma(u, v)$  and  $I(\theta_x, \theta_y)$  are Fourier transform pairs. Of course, a reasonable estimate of  $I(\theta_x, \theta_y)$  requires adequate sampling of  $\gamma(u, v)$  in the  $u, v$  plane.

There are then four quantities that are observed during a single source-baseline epoch. They are the interferometer delay, cross-correlation amplitude and phase, and the phase time rate of change. The fringe rate is

$$\dot{\phi} = \frac{\partial \phi}{\partial t} = - B \Omega \cos D \cos \delta \sin L,$$

where  $\Omega$  is the sidereal rotation rate of the earth. Fringe rates are typically several hundred Hertz for baselines of  $10^6$  wavelengths.

#### B. Very Long Baseline Interferometry

To properly measure the spatial coherence across the radiation field of a very small angular diameter source,  $\ll 10''$ , large sampling separations are required, i.e.,  $> 10^6$  wavelengths. Real time, phase stable transmissions of each observatory's sampled video data to a remote cross-correlator present a technical difficulty as yet not overcome in a practical manner. Although two-element long baseline interferometers have been linked through relay satellites, thus far it is prohibitively expensive. The standard practice today is based upon individual station local oscillators with state-of-the-art phase stability, high data density tape recorders and sophisticated hardware/software devices calculating cross-correlation between pairs of data tapes. Several tape recorder VLBI systems are presently in use. The NRAO Mark I VLBI system writes sampled video data on standard 9 track tapes in IBM-compatible format. The widest MkI bandwidth is 360 kHz. The low data rates of the MkI make for very few data errors and high accuracy in the calculation of cross-correlation amplitude and phase. Data processing of MkI tapes are accomplished entirely in software and can be done on any suitably large computer. The primary disadvantage to the MkI system, besides requiring prodigious amounts of computer time, is

its relatively narrow bandwidth. The MkI was the first VLBI recording system in general use and is maintained today for observations requiring accurate interferometer phase, such as source-position measurements. The NRAO Mark II VLBI system takes advantage of higher data recording rates available on commercial helical-scan video tape recorders. The maximum video bandwidth possible with the MkII is 2 MHz. Cross-correlation calculations, tracking incremental delay and fringe stopping are accomplished in a hardware/software device, the MkII VLBI Processor. General purpose computer usage is drastically reduced by the MkII Processor. Although the wider bandwidths result in increased S/N on the cross-correlation samples, interpretation of the absolute interferometer phase is difficult. The MkII Processor can be used as a spectral line VLB correlator, that is, it calculates cross-correlation spectra,  $S(\omega_k)$ . The NRAO MkII system is in wide use today, mainly for sampling high S/N cross-correlation amplitudes of structured continuum sources, and spectral line measurements of OH and H<sub>2</sub>O masers. The MkII Record and Processor system was used in this experiment and is described in detail in Appendix C. Within the past year, the new NASA MkIII VLBI system has come into operation. The MkIII combines the best features of the MkI and MkII. A video bandwidth of up to 50 MHz is recorded in 2 MHz increments on a 25 channel instrumentation tape recorder. The MkIII is an extremely versatile instrument and offers

a factor of 5 increase in S/N over the MkII. No provisions are presently available for processing spectral line observations.

The successful operation of tape recorder and remote correlation VLBI systems depends upon four criteria.

1. The local oscillators at each station must have sufficient spectral purity and frequency accuracy such that they establish a reasonable coherence time,  $T_c$ .  $T_c$  is that time interval over which random  $L_o$  phase fluctuations degrade the cross-correlation amplitude by 0.5. That is, if the cross-correlation amplitude is a constant,  $A$ , and the temporal variations in  $L_o$  phase,  $\varphi(t)$ , the coherence time is defined such that (Moran 1977):

$$A(T_c) = \left| \left\langle \frac{1}{T_c} \int_0^{T_c} \exp[j \varphi(t)] dt \right\rangle \right| = \frac{A}{2} .$$

For randomly distributed  $\varphi(t)$  with zero mean and variance  $\sigma_\varphi^2 = \langle \varphi^2 \rangle$ ,

$$A(T) \approx \exp\left(-\frac{\sigma_\varphi^2}{2}\right) .$$

The fractional frequency stability of the  $L_o$  is specified,  $\Delta\nu/\nu$ , hence

$$\langle \varphi^2 \rangle = [(\Delta\nu/\nu) 2 \pi \nu T]^2 .$$

Local oscillator signals are phase-locked multiplications of a 5 MHz frequency standard oscillator output. Stimulated emission from the 1420.4058 MHz neutral hydrogen transition can be produced under laboratory conditions. Emission from a hydrogen maser cavity is coupled into a system of phase-locked multipliers, dividers and synthesizers which outputs the VLBI standard frequency of 5 MHz. The fractional frequency stability of hydrogen maser standards approaches  $10^{-14}$  for  $T > 100$  sec, but decreases to  $10^{-11}$  as  $T \rightarrow 0.1$  sec. Crystal oscillators with good short-term stability are usually phase locked to the hydrogen maser output. The crystal oscillator acts as a fly wheel on the hydrogen maser, thereby improving the short-term stability. At 1665 MHz we would expect the coherence time between a pair of hydrogen maser standards to be over two hours. Small differences in the oscillator frequencies would appear as a constant fringe rate offset and are easily removed before the cross-correlation operation.

2. For typical VLBI baselines of thousands of km, the interferometer observables are very sensitive to the source-baseline geometry. As seen in Part A, an incremental delay must be applied to the signal from the station the wavefront arrives at first. As it is impractical to do this in real time at the respective observatories, the delay must be applied later in the data processing. So accurate knowledge of absolute time, hence interferometer hour angle, is necessary at each station. This is accomplished using the

100 KHz navigational broadcasts of the LORAN-C network. Observatory time can be synchronized to within  $\sim 5 \mu\text{sec}$  of UTC by the LORAN-C transmissions, quite adequate for VLBI purposes.

3. To attain reasonable S/N in cross-correlation, as wide bandwidths as possible must be sampled and recorded. A fundamental difficulty in tape recording video signals is the sheer volume of information to be recorded. In the NRAO MkII VLBI Record Terminal, video data of 2 MHz maximum bandwidth are one-bit sampled, formatted and recorded at a 4 MHz bit rate on color-television video tape recorders. The information density on the video tape is  $\approx 800 \text{ bits/mm}^2$ , typical of a photographic plate. The record terminal formats the data into frames of 1/60 second, one rotation of the record head on the helical scan recorder synchronized to station time. A 4 MHz signal from the station frequency standard is diphase encoded into the data stream as an 'assured' clock. A complete time code is written on the audio track at 1/60 sec intervals. In this way, the UTC of a single data bit can be recovered at playback by reading the time code, counting frames from the last UTC second and counting bits in the assured clock.

4. The MkII VLB Processor, located at the NRAO, Charlottesville, Virginia, is a hardware/software device which plays back tapes from pairs of stations and calculates the appropriate cross-correlation functions. The MkII Processor is discussed in detail in Appendix B. The MkII is a very versatile instrument allowing entry

of offsets in  $\omega_{LO}$ ,  $\tau_g$ , and baseline-source geometry. The MkII reduces the number of data bits per second by a factor of  $\sim 3600$ .

Observations of a particular source at a set of observing parameters are conducted over a contiguous length of time called an observing scan. In the spectral line mode, MkII observing scans are typically 50 minutes on-source followed by a 5 minute off-source scan. The MkII Processor correlates at a real-time rate filling a 9 track computer tape in approximately 55 minutes.

#### C. Uncertainties in the Cross-Correlation Vector

The observed cross-correlation is a complex quantity,  $R e^{j\phi}$ , which is the sum of the signal cross-correlation and randomly distributed noise vectors,  $R e^{j\phi} = \sum_{i=1}^N A_i e^{j\theta_i}$ . The expectations and variances in  $R$  and  $\phi$  can be estimated using the theory of random phasor sums. Consider the signals from each interferometer element that are input to the cross-correlator,

$$x_1(t) = \sqrt{T_{A1}} S_1(t) + \sqrt{T_{R1}} n_1(t) \quad ,$$

$$x_2(t) = \sqrt{T_{A2}} S_2(t) + \sqrt{T_{R2}} n_2(t) \quad .$$

$T_{A1}$  and  $T_{A2}$  are the antenna temperatures of a point source,  $T_{R1}$  and  $T_{R2}$  are the system temperatures, and  $S_1(t)$ ,  $S_2(t)$ ,  $n_1(t)$  and  $n_2(t)$  are the time representations of the statistical fluctuations in the

antenna and noise signals with normalized variance and zero mean.

The cross-correlation is

$$\begin{aligned} R(t) &= x_1^+(t)x_2(t) \\ &= \sqrt{T_{A1}T_{A2}} s_1^+(t)s_2(t) + \sqrt{T_{A1}T_{R2}} s_1^+(t)n_2(t) \\ &\quad + \sqrt{T_{A2}T_{R1}} s_2^+(t)n_1(t) + \sqrt{T_{R1}T_{R2}} n_1^+(t)n_2(t) \end{aligned}$$

where the expectations of the various conjugate products of the  $S(t)$ 's and  $n(t)$ 's are unity. The true cross-correlation is the vector

$$C e^{j\phi} = \sqrt{T_{A1}T_{A2}} s_1^+(t)s_2(t)$$

The remaining terms in  $R(t)$  are uncorrelated and statistically independent, thus summing to a single noise vector with randomly distributed phases (Rogers 1977). Then the measured cross-correlation is the vector sum

$$\bar{R} = \bar{C} + \bar{n}_1 + \bar{n}_2 = \bar{C} + \bar{n}$$

where

$$\begin{aligned} n_1 &= \sqrt{\frac{T_{A1}T_{A2}}{\Delta\nu\tau_c}} e^{j\phi} \\ n_2 &= \sqrt{\frac{T_{A1}T_{R2} + T_{A2}T_{R1} + T_{R1}T_{R2}}{\Delta\nu\tau_c}} e^{j\theta} \end{aligned}$$

where  $n_1$  is the rms of the statistical fluctuations in  $C$  and lies in the direction of  $C$  and  $n_2$  is the rms of the statistically independent cross-correlation terms. For a 128 channel Hanning weighted cross-correlation spectrum, the frequency resolution is  $\Delta\nu = 4 B/128$  with bandwidth  $B$ . The  $\tau_c$  is the coherent integration interval.

If the phase of  $C$  is defined as zero,  $C_x = C$  and  $C_y = 0$ , the quadrature components of the  $\bar{n}_1 + \bar{n}_2$  variance can be simply expressed (Moran 1976b),

$$\begin{aligned} \sigma_x^2 &= [(T_{A1} + T_{R1})(T_{A2} + T_{R2}) + T_{A1}T_{A2}]/2 \Delta\nu\tau_c \\ \sigma_y^2 &= [(T_{A1} + T_{R1})(T_{A2} + T_{R2}) - T_{A1}T_{A2}]/2 \Delta\nu\tau_c \end{aligned}$$

The vector diagram of  $\bar{R} = \bar{C} + \bar{n}_1 + \bar{n}_2$  is shown in Figure A.3.

Generally  $n_1(t) \ll n_2(t)$ , hence  $\sigma_x \approx \sigma_y$  and the total noise vector can be considered as a uniformly distributed phasor. The phase distribution is uniform,

$$P(\theta) = \frac{1}{2\pi} \quad (0 \leq \theta \leq 2\pi)$$

and the amplitude distribution

$$P(n) = \frac{n}{\sigma_x \sigma_y} \exp(-n^2/2 \sigma_x \sigma_y)$$

is the Rayleigh distribution. The distribution of the quadrature components of R is that of a constant phasor plus a Rayleigh phasor (Beckmann 1967):

$$P(R_x, R_y) = \frac{1}{2\pi \sigma_x \sigma_y} \exp\left[-\frac{(R_x - C)^2}{2\sigma_x^2} - \frac{R_y^2}{2\sigma_y^2}\right]$$

The amplitude and phase distributions of the measured cross-correlation are written (Beckmann 1967):

$$P(R) = \frac{R}{\sigma_x \sigma_y} \exp\left[-\frac{R^2 + C^2}{2\sigma_x \sigma_y}\right] I_0\left(\frac{RC}{\sigma_x \sigma_y}\right)$$

where  $I_0(z)$  is the modified Bessel function of zero order

$$I_0(z) = \frac{1}{2\pi} \int_0^{2\pi} \exp(z \cos \psi) d\psi$$

and

$$P(\phi) = \frac{1}{2\pi} \exp\left(-\frac{C^2}{2\sigma_x \sigma_y}\right) \left[1 + G \sqrt{\pi} (1 + \operatorname{erf} G) \exp G^2\right]$$

where

$$G = \frac{C \cos \phi}{\sqrt{2\sigma_x \sigma_y}} \quad (0 \leq \phi \leq 2\pi)$$

For the strong signal case,  $T_{A1} T_{A2} \gg T_{R1} T_{R2} / 2 \Delta \nu \tau_c$ , the expectations and variances of R and  $\phi$  can be estimated (Moran 1977):

$$\langle R \rangle \approx \sqrt{T_{A1} T_{A2}} \left(1 + \frac{T_{R1} T_{R2}}{4 T_{A1} T_{A2} \Delta \nu \tau_c}\right)$$

$$\sigma^2 \approx \frac{T_{R1} T_{R2}}{2 \Delta \nu \tau_c}$$

$$\langle \phi \rangle = 0$$

$$\sigma_\phi^2 \approx \frac{T_{R1} T_{R2}}{2 T_{A1} T_{A2} \Delta \nu \tau_c}$$

The strong signal approximation is a valid case for this experiment

where  $T_{A1} T_{A2} \approx 1 \text{ } ^\circ\text{K}^2$  for weak features (5 Jy) and typically

$$T_{R1} T_{R2} / 2 \Delta \nu \tau_c \approx 0.1 \text{ } ^\circ\text{K}^2.$$

If  $N$  consecutive samples of  $\phi$  determine the fringe rate,  $\dot{\phi}$ , the error in  $\dot{\phi}$  is

$$\sigma_{\dot{\phi}} = \frac{\sqrt{12} \sigma_{\phi}}{\tau_c [N(N+1)(N-1)]^{1/2}}$$

For the weak signal case,  $\sqrt{T_{A1} T_{A2}} \ll \sqrt{T_{R1} T_{R2}} / \sqrt{2 \Delta \nu \tau_c}$ ,

$$\langle R \rangle \approx \left(\frac{\pi}{2}\right)^{1/2} \sqrt{\frac{T_{R1} T_{R2}}{2 \Delta \nu \tau_c}} \left(1 + \frac{T_{A1} T_{A2}}{T_{R1} T_{R2}} \cdot \frac{\Delta \nu \tau_c}{2}\right),$$

$$\sigma^2 \approx \frac{T_{R1} T_{R2}}{2 \Delta \nu \tau_c} \left(2 - \frac{\pi}{2}\right) \left(1 + \frac{T_{A1} T_{A2}}{T_{R1} T_{R2}} \cdot \frac{\Delta \nu \tau_c}{2}\right)^2,$$

$$\langle \dot{\phi} \rangle = 0,$$

$$\sigma_{\dot{\phi}}^2 \approx \frac{\pi^2}{3} \left(1 - \left(\frac{9}{2\pi^3}\right)^{1/2} \frac{T_{A1} T_{A2}}{T_{R1} T_{R2}} \cdot 2 \Delta \nu \tau_c\right)^2$$

as  $T_{A1} T_{A2} \rightarrow 0$ ,

$$\langle R \rangle = \left(\frac{\pi}{2}\right)^{1/2} \sqrt{\frac{T_{R1} T_{R2}}{2 \Delta \nu \tau_c}} ; \quad \sigma^2 = \frac{T_{R1} T_{R2}}{2 \Delta \nu \tau_c} \left(2 - \frac{\pi}{2}\right) ;$$

$$\sigma_{\dot{\phi}}^2 = \frac{\pi^2}{3}$$

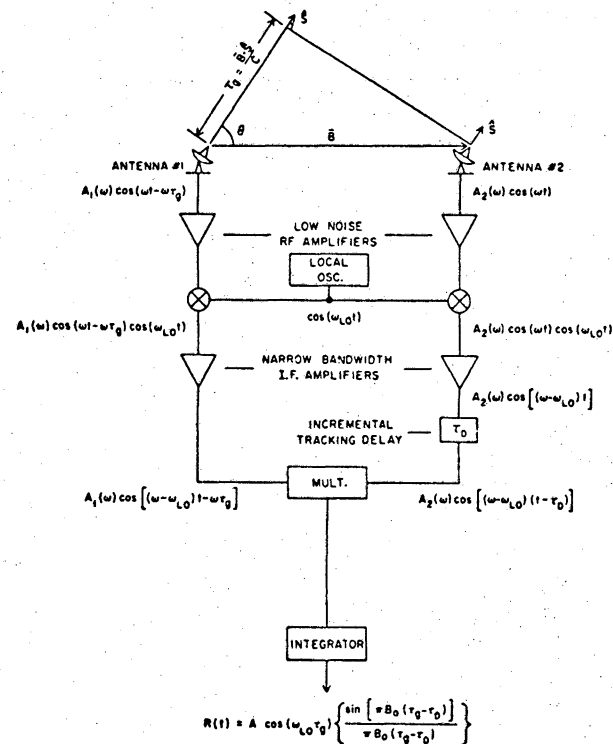
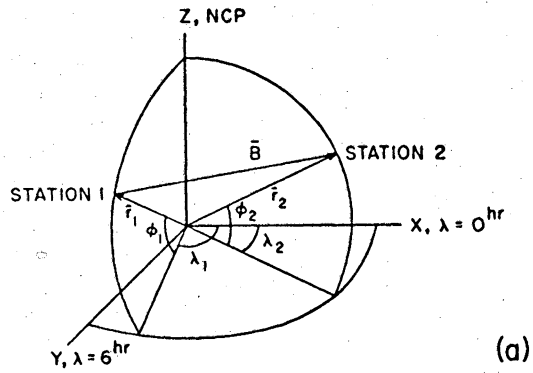
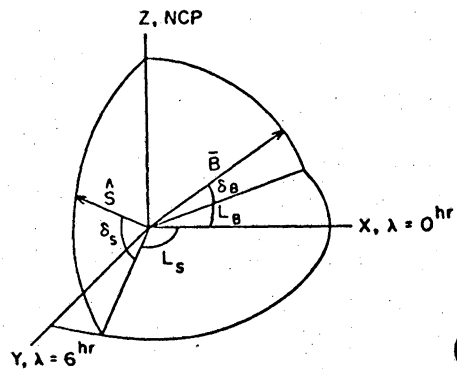


Figure A.1. Schematic representation of a simple connected-element multiplying interferometer. The incremental tracking delay inserts a delay in signal #2 equivalent to the geometrical delay in signal #1. The bandpass has a rectangular frequency response from 0 to  $B_0$  Hz, hence the interferometer response is of the form of  $A \cos(\omega_{LO} \tau_g)$  fringes under the  $\text{sinc}[\pi B_0 (\tau_g - \tau_D)]$  delay tracking offset window.

A-678-573



(a)



(b)

Figure A.2. Radio source - interferometer baseline geometry.  
 (a) An interferometer baseline vector in terms of the geocentric coordinates of the observing stations. The  $x$ ,  $y$  lie in the equatorial plane with  $x$  in the direction of the Greenwich Meridian;  $z$  is toward the North Celestial Pole.  
 (b) Source direction and interferometer baseline vectors expressed in terms of declinations and Greenwich Hour Angles. The  $x$ ,  $y$ ,  $z$  coordinates are the same as in (a).

A-678-712

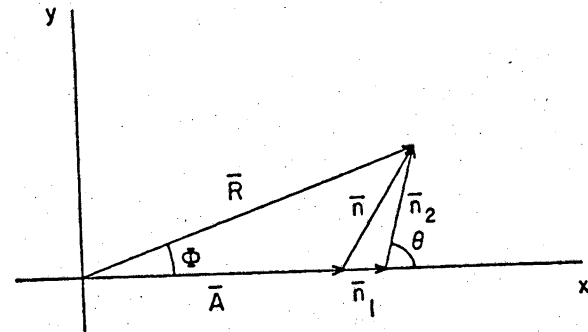


Figure A.3. The observed cross-correlation phasor  $\bar{R}$  is the vector sum of three vectors in cross-correlation space.  $\bar{A}$  is the true interferometer cross-correlation,  $\bar{n}_1$  is the rms of the statistical fluctuations in  $\bar{A}$ , and  $\bar{n}_2$  is a Rayleigh phasor proportional to the mean interferometer system temperature. In this example,  $\bar{A}$ , and hence  $\bar{n}_1$ , are constrained to have zero phase angle.

## APPENDIX B

## A COMPENDIUM OF VLBI FORMULAE

A. Glossary of Parameters

The nomenclature of coordinates and parameters used in this thesis and in this appendix are as follows:

B	:	Baseline in units of wavelength
$B_{EQ}$	:	Equatorial component of B
$L_B, \delta_B$	:	Baseline GHA (Greenwich Hour Angle) and declination
$\varphi'_i, \lambda'_i$	:	Geocentric latitude and longitude of the $i^{th}$ station
$R_i$	:	Geocentric radius at $\varphi'_i, \lambda'_i$
$\varphi_i, \lambda_i$	:	Geodetic latitude and longitude of the $i^{th}$ station
$\alpha_s, \delta_s$	:	Source right ascension and declination
$L_s$	:	Source GHA
$\theta_i, L_{si}$	:	Source elevation and hour angle as viewed from $i^{th}$ station

$\theta_x, \theta_y$	:	Source position offsets from $\alpha_s, \delta_s$
$\Omega$	:	Sidereal angular rotation velocity of earth
UT	:	Universal Coordinated Time
$\omega$	:	Observing frequency
GST	:	Right ascension at meridian transit at 0 hours UT at $\lambda' = 0$ hours.

B. Baseline Geometry: Geodetic to Geocentric Conversion

$$\lambda' = \lambda$$

$$\varphi' - \varphi = -11' 32'' 7430 \sin 2 \varphi + 1'' 1633 \sin 4 \varphi - 0'' 0026 \sin 6 \varphi$$

The geocentric radius is

$$R = \frac{a}{\lambda} (0.998327073 + 0.001676438 \cos 2 \varphi - 0.000003519 \cos 4 \varphi + 0.000000008 \cos 6 \varphi)$$

where the equatorial radius

$$a = 6378.160 \text{ km}$$

In the geocentric coordinate system,  $x = 0$  hrs GHA,  $y = 6$  hrs GHA and  $z = \delta = 90^\circ$ , the position of the  $i^{th}$  station is

$$\begin{bmatrix} x_i \\ y_i \\ z_i \end{bmatrix} = R_i \begin{bmatrix} \cos \varphi'_i \cos \lambda'_i \\ \cos \varphi'_i \sin \lambda'_i \\ \sin \varphi'_i \end{bmatrix}$$

The baseline vector is defined as the vector pointing from station #1 (western) to station #2 (eastern) in the geocentric coordinate system, that is

$$\begin{aligned} \bar{B} &= \bar{R}_2 - \bar{R}_1, \\ &= BX \hat{x} + BY \hat{y} + BZ \hat{z}, \end{aligned}$$

$$\begin{bmatrix} BX \\ BY \\ BZ \end{bmatrix} = \sum_{i=1}^2 (-1)^i R_i \begin{bmatrix} \cos \varphi'_i \cos \lambda'_i \\ \cos \varphi'_i \sin \lambda'_i \\ \sin \varphi'_i \end{bmatrix}$$

$$B = (BX^2 + BY^2 + BZ^2)^{1/2},$$

$$\delta_B = \sin^{-1} (BZ/B),$$

$$L_B = \tan^{-1} (BY/BX)$$

or

$$\begin{bmatrix} BX \\ BY \\ BZ \end{bmatrix} = B \begin{bmatrix} \cos \delta_B \cos L_B \\ \cos \delta_B \sin L_B \\ \sin \delta_B \end{bmatrix}$$

### C. Baseline-Source Geometry

The source GHA is

$$L_s = \text{GST} + 1.0027379093 \text{ UT} - \alpha_s$$

and interferometer hour angle is

$$L = L_s - L_B$$

The baseline vector can be reduced to the u, v, w coordinate system, where u, v is the plane parallel to the wavefronts arriving from the source and w is toward the source position,  $\alpha_s, \delta_s$ . Increasing u is towards the east and increasing v is towards the north.

$$\begin{bmatrix} u \\ v \\ w \end{bmatrix} = \begin{bmatrix} \sin L_s & -\cos L_s & 0 \\ \sin \delta_s \cos L_s & -\sin \delta_s \sin L_s \cos \delta_s \\ \cos \delta_s \cos L_s & \cos \delta_s \sin L_s \sin \delta_s \end{bmatrix} \begin{bmatrix} BX \\ BY \\ BZ \end{bmatrix}$$

or

$$u = B \cos \delta_B \sin L ,$$

$$v = B(\sin \delta_B \cos \delta_S - \cos \delta_B \sin \delta_S \cos L) ,$$

$$w = \bar{B} \cdot \hat{s} = B(\sin \delta_B \sin \delta_S + \cos \delta_B \cos \delta_S \cos L) ,$$

then

$$u_{MAX} = B_{EQ} ,$$

$$v_{MAX} = B \cos \delta_S + u_{MAX} \sin \delta_S .$$

The baseline track in  $u, v$  with changing interferometer hour angle is

$$u = a \sin L ,$$

$$v = v_0 - b \cos L ,$$

which over 24 hours describes the ellipse

$$\frac{u^2}{a^2} + \frac{(v - v_0)^2}{b^2} = 1 ,$$

where

$$a = B \cos \delta_B ,$$

$$b = B \cos \delta_B \sin \delta_S ,$$

$$v_0 = B \sin \delta_B \cos \delta_S .$$

#### D. The Interferometer Observables

##### 1. Time Delay

$$\tau = \frac{\lambda}{c} B \cdot \hat{s} ,$$

$$= \frac{B\lambda}{c} (\sin \delta_B \sin \delta_S + \cos \delta_B \cos \delta_S \cos L) .$$

##### 2. Fringe Phase and Rate

$$\phi = \omega \tau ,$$

$$\dot{\phi} = \omega \frac{\partial \tau}{\partial t} = \omega \frac{\partial \tau}{\partial L} \cdot \frac{\partial L}{\partial t} ,$$

$$\dot{\phi} = -2\pi \Omega u \cos \delta_B \cos \delta_S \sin L ,$$

$$= -2\pi \Omega u \cos \delta_S ,$$

where  $\Omega$  is sidereal angular velocity of the earth,  $\Omega = 1.160576(10)^{-5}$  sidereal Hz.

## 3. Complex Visibility

$$\gamma(u,v) = \int_{-\infty}^{\infty} \int_{-\infty}^{\infty} d\theta_x d\theta_y I(\theta_x, \theta_y) \cdot \exp[j 2 \pi (u\theta_x + v\theta_y)]$$

where  $I(\theta_x, \theta_y)$  is source brightness distribution.

## E. Offsets in Observables

Offsets in the parameters which describe source-baseline geometry result in interferometer observables other than would be predicted. If the offsets are small, they may be conveniently expressed as incremental changes in the spherical coordinates of the baseline or source position. Using Taylor expansions of the observables in terms of the offset parameters, the changes in  $\tau$ ,  $\phi$  and  $\delta$  have been calculated.

## 1. Source Position Offsets

If the source position offsets are defined as

$$a_x = (\alpha - \alpha_s) \cos \delta_s ,$$

$$a_y = \delta - \delta_s ,$$

then the observable offsets are (Moran 1976b):

$$\Delta\tau = \frac{\lambda}{c} (u\theta_x + v\theta_y) ,$$

$$\Delta\phi = 2 \pi (u\theta_x + v\theta_y) ,$$

$$\Delta\delta = 2 \pi \Omega B_{EQ} (\cos L \cdot \theta_x + \sin \delta_s \sin L \cdot \theta_y) .$$

## 2. Baseline Offsets

Consider baseline offsets specified in geocentric coordinates.

$$\Delta BX = BX - BX_0$$

$$\Delta BY = BY - BY_0$$

$$\Delta BZ = BZ - BZ_0$$

where  $B_0 = [BX_0^2 + BY_0^2 + BZ_0^2]^{1/2}$  is the reference baseline, i.e., used in the MkII Processor, Figure B-1.

Expanding and disregarding terms 2nd order and higher in  $\Delta BX$ ,  $\Delta BY$  and  $\Delta BZ$ , the offsets may be expressed in terms of baseline direction and length.

$$\Delta B_{EQ} = (\Delta BX \cdot BX_0 + \Delta BY \cdot BY_0) / B_{0,EQ} ,$$

$$\Delta B = (\Delta BX \cdot BX_0 + \Delta BY \cdot BY_0 + \Delta BZ \cdot BZ_0) / B_0 ,$$

$$\Delta L_B = (\Delta BY \cdot BX_0 - \Delta BX \cdot BY_0) / B_{0,EQ}^2 ,$$

$$\Delta \delta_B = (\Delta BZ \cdot B_{0,EQ} - \Delta B_{EQ} \cdot BZ_0) / B_0^2 ,$$

then

$$\Delta\tau = \frac{\lambda B_0}{c} \{ [\sin \delta_B \sin \delta_S + \cos \delta_B \cos \delta_S \cos L] \cdot \frac{\Delta B}{B_0} + [\cos \delta_B \cos \delta_S \sin L] \cdot \Delta L_B + [\cos \delta_B \sin \delta_S - \sin \delta_B \cos \delta_S \cos L] \cdot \Delta \delta_B \} ,$$

$$\Delta \dot{\phi} = \omega \Delta\tau ,$$

$$\Delta \dot{\delta} = 2 \pi \Omega B_{O, EQ} \cos \delta_S \left( \cos L \cdot \Delta L_B - \sin L \cdot \frac{\Delta B_{EQ}}{B_{O, EQ}} \right) .$$

In the case of an equationally mounted telescope whose hour angle and declination axis do not intersect, but are connected by a vector,  $\bar{b}$ , which is orthogonal to both, the vector  $\bar{b}$  then is in the equational plane and points toward the source right ascension. Its GHA is the source GHA,  $L_S$ , and the angle  $\bar{b}$  makes with  $\bar{B}_{EQ}$  is in fact  $L$ . Therefore, the baseline offsets are simply

$$\Delta B_{EQ} = b \cos L ,$$

$$\Delta B = b \frac{B_{O, EQ}}{B_0} \cos L ,$$

$$\Delta L_B = \frac{b}{B_{O, EQ}} \sin L ,$$

$$\Delta \delta_B = 0 .$$

Note that  $\Delta \dot{\delta} = 0$  for this case.

### 3. Time Offsets

If  $GST_0$  and  $UT_0$  are the reference times, then

$$\Delta L_T = (GST - GST_0) + 1.0027379 (UT - UT_0)$$

and

$$\Delta\tau = \frac{\lambda B_0}{c} \cos \delta_B \cos \delta_S \sin L \cdot \Delta L_T ,$$

$$\Delta \dot{\phi} = \omega \Delta\tau ,$$

$$\Delta \dot{\delta} = - 2 \pi \Omega B_{O, EQ} \cos \delta_S \cos L \cdot \Delta L_T .$$

### 4. Differential Atmospheric Delay

The group delay due to the index of refraction of the neutral atmosphere is expressed by a simple model with an accuracy of 10% to 15% (Robertson 1975):

$$\tau_A(\theta_i) = \tau_z \left[ \sin \theta_i + \frac{0.00145}{\tan \theta_i + 0.0445} \right]^{-1} ,$$

where  $\tau_z$  is the delay through the atmosphere towards the zenith and  $\theta_i$  is the source elevation angle at the  $i^{\text{th}}$  station,

$$\tau_z = 7(10)^{-9} \text{ sec} ,$$

$$\theta_i = \frac{\pi}{2} - \cos^{-1} (\sin \varphi'_i \sin \delta_s + \cos \varphi'_i \cos \delta_s \cos L_{si})$$

and

$$L_{si} = \text{GST} + 1.0027379 \text{ UT} - \alpha_s - \lambda'_i .$$

The observable offsets become

$$\Delta\tau = \tau_A(\theta_1) - \tau_A(\theta_2) ,$$

$$\Delta\dot{\phi} = \omega\Delta\tau ,$$

$$\Delta\dot{\phi} = \omega \frac{\partial \Delta\tau}{\partial t} = \omega \sum_{i=1}^2 (-1)^{l=i} \frac{\partial \tau(\theta_i)}{\partial \theta_i} \cdot \frac{\partial \theta_i}{\partial t} ,$$

where

$$\frac{\partial \tau(\theta_i)}{\partial \theta_i} = -\tau_0 \frac{\left[ \cos \theta_i - \frac{0.00143 \text{ sec}^2 \theta_i}{(\tan \theta_i + 0.0445)^2} \right]}{\left[ \sin \theta_i + \frac{0.00143}{\tan \theta_i + 0.0445} \right]^2}$$

$$\frac{\partial \theta_i}{\partial t} = \frac{-\frac{\omega}{c} \Omega_B \cos \varphi'_i \cos \delta_s \sin L_{si}}{\left[ 1 - (\sin \varphi'_i \sin \delta_s + \cos \varphi'_i \cos \delta_s \cos L_{si})^2 \right]^{1/2}}$$

### 5. Diurnal Aberration

The angular rotational velocity of the earth causes the interferometer delay to be shortened or lengthened as  $L$  increases. A dimensionless correction factor is determined as a function of the coordinates of the station at which the source wavefronts arrive late (Cohen and Shaffer 1971), such that

$$\Delta\tau = \epsilon_i \tau_i ,$$

$$\Delta\dot{\phi} = \omega\Delta\tau ,$$

$$\Delta\dot{\phi} = \epsilon_i \dot{\phi} + \omega\tau\dot{\epsilon} ,$$

where

$$\epsilon_i = -\frac{\Omega R_i}{c} \cos \varphi'_i \cos \delta_s \sin L_{si} ,$$

$$\dot{\epsilon}_i = -\frac{\Omega^2 R_i}{c} \cos \varphi'_i \cos \delta_s L_{si}$$

and

$$i = 1 \text{ (western station) when } \tau > 0$$

$$i = 2 \text{ (eastern station) when } \tau < 0 .$$

A-678-574

APPENDIX C

FUNDAMENTALS OF THE NRAO MkII VLB RECORD  
AND PLAYBACK SYSTEM

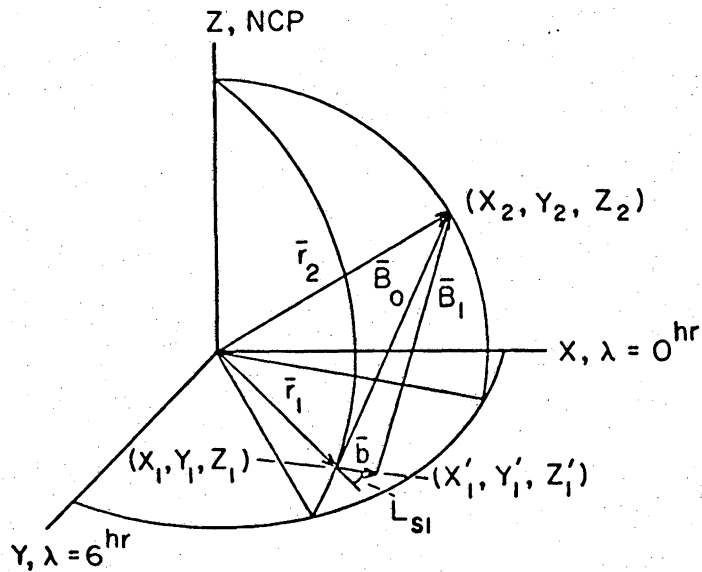


Figure B.1. The true interferometer baseline,  $\bar{B}_1$ , is the vector sum of the specified interferometer baseline,  $\bar{B}_0$ , and a small offset geocentric position of station #1,  $\bar{b}$ . The local hour angle of  $\bar{b}$  at  $X_1, Y_1, Z_1$  is  $L_{s1}$ . In this case, the declination of  $\bar{b}$  is zero.

This appendix discusses the NRAO MkII operation in terms of the major hardware and software components along the respective signal paths. Phase, frequency and time errors introduced during observations and subsequent processing are reduced to the resultant offsets in the processor output. Expressions for the signals from each antenna are traced through the MkII system with particular attention given to the fringe phase. A detailed description of the MkII operation is presented by Clark (1974) and an overall review of VLBI correlators, including the MkII, by Moran (1976b).

A. MkII VLB Record System

Phase stable video signals will be recorded at station #1 (western) and station #2 (eastern), see Figure C.1. The various multiple mixing schemes at different VLB observatories can be conveniently expressed as one SSB mixer to which is applied  $\omega_{LO}$ , the 0 Hz video frequency. The signals at each station preceding the SSB are:

$$x_1(t) = S_1(\omega)G_1(\omega)\cos[\omega t - \omega\tau_g + \varphi_1(t) + \psi_1(\omega)] ,$$

$$x_2(t) = S_2(\omega)G_2(\omega)\cos[\omega t + \varphi_2(t) + \psi_2(\omega)] ,$$

where

$\omega$  = observing frequency,

$S_i(\omega)$  = sky signal at station  $i$ ,

$G_i(\omega)$  = total gain through station  $i$ ,

$\varphi_i(t), \psi_i(\omega)$  = time and frequency dependent phase offsets at station  $i$ ,

$t$  = epoch defined as the arrival of  $\omega = \omega t$  at station #2.

The actual geometric time delay is

$$\tau_g = \tau_{go}(\text{calc. from } \frac{\lambda \bar{B} \cdot \hat{s}}{c}) + \Delta\tau_g .$$

The term  $\Delta\tau_g$  is the sum of contributions from differential tropospheric delay, diurnal aberration, errors in specifying the source-baseline geometry, relativistic effects and frequency dependent propagation delays.

The local oscillator signal of the  $i^{\text{th}}$  station is  $\cos[\omega'_{LOi} t + \varphi_{Li}(t)]$ . The RF signal is mixed to baseband, USB

selected and low pass filtered such that  $0 \leq (\omega - \omega'_{LO}) \leq 2\pi B_o$ .

The applied LO frequency is  $\omega'_{LO1}$ , the specified LO frequency is  $\omega_{LO1}$ , phase offsets in the LO are  $\varphi_{L1}(t)$ , and the video bandwidth is  $B_o$ . The video signals to the MkII sampler input are:

$$x_1(t) = S_1(\omega)G_1(\omega)\cos[(\omega - \omega'_{LO1})t - \omega\tau_g + \varphi_1(t) + \psi_1(\omega)] ,$$

$$x_2(t) = S_2(\omega)G_2(\omega)\cos[(\omega - \omega'_{LO2})t + \varphi_2(t) + \psi_2(\omega)] ,$$

where the LO and sky phase offsets are combined in  $\varphi_i(t)$ .

In the MkII, the video signal is one-bit sampled at a 4 MHz rate and diphase encoded with 4 MHz derived from the station frequency standard. The station timing superimposed on the video data stream is the assured clock. The data are organized into 1/60 sec records (frames) with 8 bit synch words every 512  $\mu$ sec. One frame is recorded on each pass of the rotating head on the helical-scan video tape recorder. A station clock offset from UTC,  $\tau_{c1}$ , introduces a phase slope across the video passband recorded by the MkII:

$$x_1(t) = S_1(\omega)G_1(\omega)\cos[(\omega - \omega'_{LO1})t - \omega\tau_g + (\omega - \omega'_{LO1})\tau_{c1} + \varphi_1(t) + \psi_1(\omega)] ,$$

$$x_2(t) = S_2(\omega)G_2(\omega)\cos[(\omega - \omega'_{LO2})t + (\omega - \omega'_{LO2})\tau_{c2} + \varphi_2(t) + \psi_2(\omega)] .$$

### B. MkII VLE Playback System

The recorded video tapes from all stations are brought together at the site of the MkII VLE Processor at NRAO, Charlottesville, Virginia. The proper interferometer delay and fringe rates at the observing epoch are calculated in the on-line Varian 620 computer and by means of hardware/software combinations are applied to the appropriate data streams. One, two or three baselines may be processed simultaneously with various combinations of length of complex cross-correlation and autocorrelation functions totaling 576 correlation channels. We will consider here the case of correlating over a single baseline in the spectral line mode.

The processing sequence begins with the MkII hardware reading the time codes and frame counts on each tape and aligning the playback recorders (refer to Figure C.2). The phase of the rotating head drums of each recorder are controlled by the MkII such that temporal alignment is maintained. The sampled video data and the assured clocks are recovered from each stream of encoded data. The sampled video data are sequentially loaded bit by bit into 2048 bit ring buffers. The individual bit address, the load pointer address (LPA), is the count of the assured clock from the preceeding synch word. Since the assured clock phase is sensitive to the recorder instabilities,  $\sim 100 \mu\text{sec}$ , the sampled video data is not loaded into the delay buffer at a uniform rate. The address of the unload

pointer (ULPA) for each delay buffer is the count of pulses from a single 4 MHz crystal oscillator. Thus the data streams from each delay buffer emerge at a uniform rate. The playback recorder head drums are phase locked to a 60 Hz waveform from the ULPA counter. Therefore, within the limits of the head drum control,  $\sim 100 \mu\text{sec}$ , the ULPA and head drum rates are synchronous. The synch words recorded at 512  $\mu\text{sec}$  intervals in the data stream are used to reset the LPA. If the LPA is not zero when a synch word appears, the LPA is reset and the MkII indicates a data dropout. Since the ULPA increments at a uniform rate whereas the LPA has the 100  $\mu\text{sec}$  recorder fluctuations, and as the ring buffer is cycled in 512  $\mu\text{sec}$ , the ULPA must follow the LPA by approximately 180 degrees to avoid overwritten data. The delay calculated by the Varian 620 is inserted into the data stream of which the source wavefront arrives first. The Varian 620 drops pulses in the 4 MHz to the ULPA counter, thereby delaying the ULPA and hence its recorder's head drum. The LPA sees the playback recorder slowing through the assured clock. The  $\sim 180$  degree phase difference between the LPA and ULPA is maintained as the recorder reaches the calculated delay. Small changes in delay are accomplished mainly in the delay buffer. Station time is determined from the time code track, the frame count and the assured clock count following the synch words.

As defined in Section A, the source wavefront is delayed to station #1. The processor will delay the data stream from station #2:

$$x_2(t) = A_2(\omega) \cos[(\omega - \omega'_{L02})(t + \tau_{c2}) - (\omega - \omega'_{L02})\tau_p + \psi_2(t) + \psi_2(\omega)]$$

The processor delay,  $\tau_p$ , tracks the geometrical delay,  $\tau_{go}$ , in increments of  $1/2B_0$  thereby introducing a delay error in data stream #2:

$$\Delta\tau_p = \tau_p - \tau_{go}$$

Observations at centrimetric wavelengths over interferometer baselines of several thousand kilometers produce fringe rates in the kHz. In order to reduce the data processing rate and increase the correlator integration time, the high natural fringe rate is removed by the lobe rotator. In the lobe rotator, one data stream is multiplied in quadrature by the phase of artificial fringes whose rate and phase are calculated by the Varian 620 for that epoch. The lobe rotator acts as a SSB mixer in that the fringe frequencies are reduced to baseband. The artificial fringes are generated from 4 MHz by the Varian controlled programmable divider. The phase and rate are updated every 0.1 sec and the fringe rate period is tracked in increments of 50 psec (Moran 1976b). At lower centimetric wavelengths, the time derivative of the fringe rate is sufficiently low such that the residual phase drifts by a fraction of a degree

between updates. The lobe rotator phase is  $\omega = \omega_{L01} \tau_{go} - (\omega_{L02} - \omega_{L01})t + \delta$ . One component of the rotated data stream is

$$x_1(t) = A_1(\omega) \cos[(\omega - \omega'_{L01})(t + \tau_{c1}) - \omega\tau_g + \psi_1(t) + \psi_1(\omega) - (\omega_{L01} \tau_{go}) + (\omega_{L02} - \omega_{L01})t + \delta]$$

The quadrature components of  $x_1$  are correlated with  $x_2$  in the 576 channel correlator. The individual correlation channels are one-bit Exclusive-OR gates such that  $XC = \sin(\frac{\pi}{2} \rho_c)$  (Weinreb 1963). The correlator delay increment is  $\Delta\tau = 1/2B_0$ . The delay to the  $i^{\text{th}}$  XC channel is  $\tau_i = i\Delta\tau$ , where  $-63 \leq i \leq 64$ . Normalization counts are recorded for each 0.2 sec integration period. To preserve correlation amplitude, the residual fringe rate must fall within a window of  $\pm 2.5$  Hz. If  $A_1(\omega)A_2(\omega) = A_1A_2$  and  $\psi_1(\omega) = \psi_2(\omega) = \psi$  over  $B_0$ , the cross-correlation of the  $i^{\text{th}}$  channel is

$$XC_i(t_0) = A_1A_2 \exp(i\psi)W(\Delta\tau_i)$$

where  $\Delta\tau_i = \tau_R + \tau_i$ , the residual time delays and the delay to the  $i^{\text{th}}$  correlator channel,  $A_1A_2$  is the cross-correlation amplitude at  $\Delta\tau_i = 0$ ,  $\psi$  is the residual fringe phase and the bandwidth smearing is

$$W(\Delta\tau_i) = \frac{\sin(\pi B_o \Delta\tau_i)}{\pi B_o \Delta\tau_i} \exp[j \pi B_o \Delta\tau_i]$$

The cross-correlation spectrum is calculated from  $XC_1(t_o)$  by the 128 channel array processor controlled by the DGC Nova II computer,

$$S_{12}(\omega_k, t_o) = A_{12}(\omega'_k, t_o) \exp(j\phi) * S(\Delta\omega)$$

where \* denotes the convolution with the spectral smearing function

$$S(\Delta\omega) = \frac{\sin\left(\frac{\pi 64 \Delta\omega}{B_o}\right)}{\frac{\pi 64 \Delta\omega}{B_o}} \exp\left[j \frac{\pi 64 \Delta\omega}{B_o}\right]$$

and  $\Delta\omega = \omega_k - \omega'_k$ . The video frequency of the  $k^{\text{th}}$  spectral channel,  $\omega_k$ , is incremented by  $B_o/128$ . The residual fringe phase in the  $k^{\text{th}}$  channel is

$$\begin{aligned} \phi = & \omega_k(\tau_g - \tau_{go} - \Delta\tau_p + \tau_{c2} - \tau_{c1}) + \omega'_{L01}(\tau_g - \tau_{go}) \\ & + (\omega'_{L02} - \omega_{L01})\tau_{go} - (\omega'_{L01} - \omega'_{L02})(\Delta\tau_p + \tau_{c2}) \\ & + ((\omega_{L02} - \omega_{L01}) - (\omega'_{L01} - \omega'_{L02}))t_o \\ & + \Delta\omega(\omega_k) + \Delta\psi(t_o) + \delta \end{aligned}$$

with  $\omega_k = \omega - \omega'_{L01}$ .

If  $\tau_{c1} = \tau_{c2}$ ,  $\tau_g = \tau_{go}$ ,  $\omega_{L01} = \omega'_{L01} = \omega_{L02} = \omega'_{L02}$ , and  $\Delta\omega = \Delta\psi = \delta = 0$ , the residual fringe phase,  $\phi = -\omega_k \Delta\tau_p$ , is a result of the incremental error in the tracking delay. This phase offset is both frequency dependent and time variable in  $\Delta\tau_p$  where  $-1/4 B_o \leq \Delta\tau_p \leq 1/4 B_o$ . Between delay increment updates,

$$\Delta t = \left[ 2 B_o \frac{d\tau_{go}}{dt} \right]^{-1}$$

the total phase rotation of the  $k^{\text{th}}$  channel is (Moran 1976b):

$$\Delta\phi_k = \frac{\omega_k}{2 B_o}$$

The Fractional Bit Shifter compensates for the error due to the discrete delay tracking by multiplying  $S_{12}(\omega_k, t_o)$  by  $\exp(j \omega_k \Delta\tau_p)$ . Thus the residual fringe phase becomes:

$$\begin{aligned}
 t &= \omega_k (\tau_g - \tau_{go} + \tau_{c2} - \tau_{c1}) + \omega'_{L01} (\tau_g - \tau_{go}) \\
 &+ (\omega'_{L02} - \omega_{L01}) \tau_{go} - (\omega'_{L01} - \omega'_{L02}) (\Delta\tau_p + \tau_{c2}) \\
 &+ ((\omega_{L02} - \omega_{L01}) - (\omega'_{L01} - \omega'_{L02})) t_o \\
 &+ \Delta\phi(\omega_k) + \Delta\psi(t_o) + \delta
 \end{aligned}$$

Errors in specifying source-baseline geometry cause  $\tau_g - \tau_{go}$  offsets. Since interferometer delay is time variable, a fringe rate offset and  $\omega_k$  dependent phase offset result. Relative clock offsets between stations also cause a phase shift across the video bandpass.

BASIC ELEMENTS OF A TYPICAL VLBI STATION

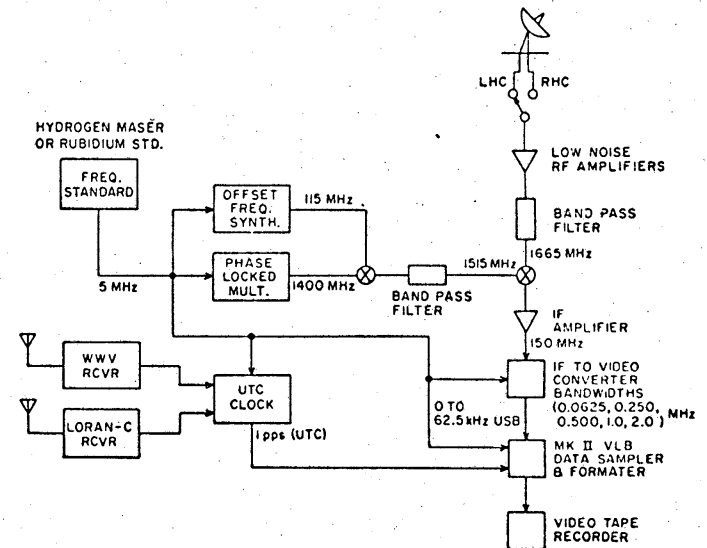


Figure C.1. The basic elements of a typical VLBI radio observatory with the local oscillator signal phase-locked to a hydrogen-maser frequency are schematically represented. The station timing is synchronized to LORAN-C UTC broadcasts and maintained within the frequency standard accuracy. The observing bandwidth is determined at baseband in the video converter. Data are sampled and formatted in the NRAO MkII VLBI Record Terminal and recorded on a modified color-television video recorder.

D-678-608

## BASIC ELEMENTS OF THE NRAO MK II VLB PROCESSOR

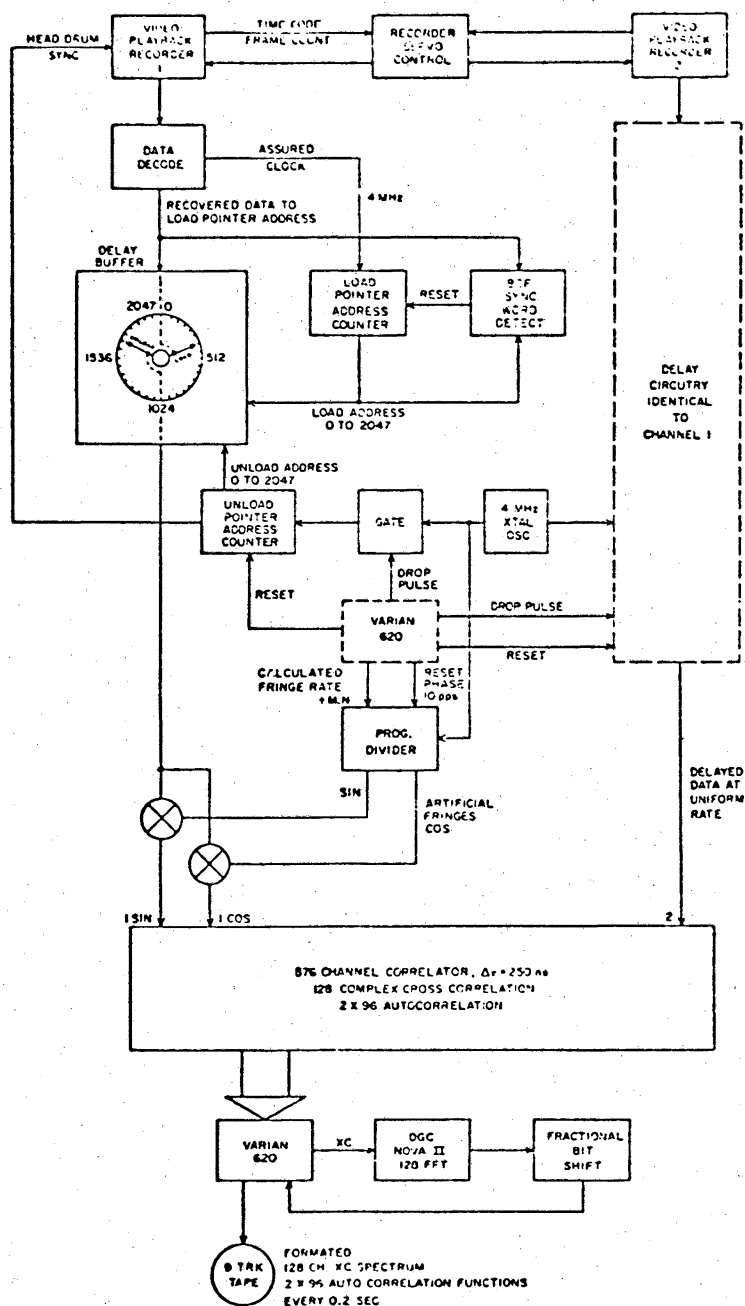


Figure C.2. Elements of the NRAO MkII VLB Processor concerned with applying incremental tracking delay, synchronizing playback recorders, and fringe lobe rotation. The Varian 620 computer reads the correlation functions at 0.2 second intervals. The DGC Nova II computer Fourier inverts the cross-correlation functions to produce cross-power spectra in real time.